Front. Agr. Sci. Eng. 2025, 12(2): 308–322

RESEARCH ARTICLE

Aeration system optimization for a deep bed dryer for paddy grain using computational fluid analysis and the AHP-TOPSIS method

Diswandi NURBA (✉)[1,2], Sutrisno S. MARDJAN[1], Dyah WULANDANI[1,3], Leopold O. NELWAN[1], I Dewa Made SUBRATA[1]

1 Department of Mechanical and Biosystem Engineering, IPB University, Bogor 16002, Indonesia.
2 Department of Agricultural Engineering, Universitas Syiah Kuala, Banda Aceh 23111, Indonesia.
3 Center for Research on Engineering Application in Tropical Agriculture (CREATA), IPB University, Bogor 16002, Indonesia.

KEYWORDS

Deep bed dryer, air aeration system, CFD, AHP-TOPSIS, paddy grain drying

HIGHLIGHTS

- Drying is a crucial postharvest process for paddy grain and impacts the quality of both paddy and rice.
- A deep bed dryer is a convective dryer that relies on airflow, temperature and relative humidity as the primary drying parameters.
- An aeration system is necessary to distribute the drying air evenly throughout the drying chamber.
- The optimal aeration system was determined using computational fluid dynamics and the AHP-TOPSIS method.
- The most optimal aeration system is a model deep bed dryer with a sloping floor and circular pipe formation.

Received March 5, 2024;
Accepted July 8, 2024.

GRAPHICAL ABSTRACT

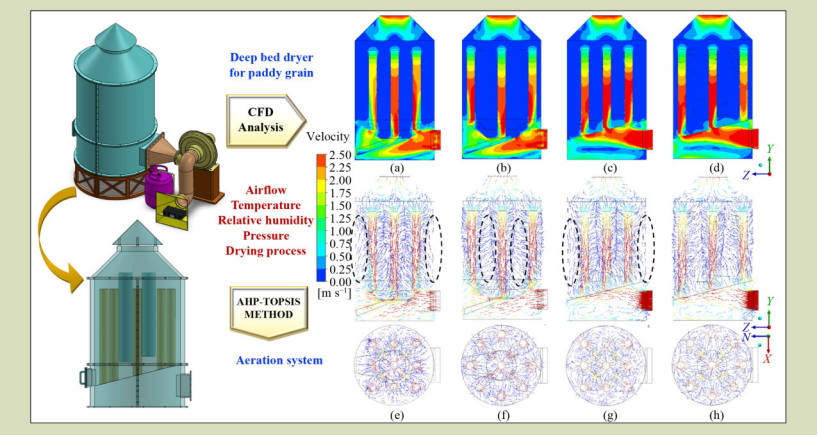

ABSTRACT

In the context of food security, drying is a crucial postharvest process for paddy grain because it significantly impacts the quality of both paddy and rice. To conserve energy during the drying process, deep bed dryers are used as convective dryers that use a combination of ambient airflow and heating, thus relying on airflow, temperature, and relative humidity (RH) as the primary drying parameters. Consequently, an aeration system is necessary so that the drying air can penetrate the thick pile of paddy grain and distribute evenly throughout the drying chamber. This analysis aimed to determine the most optimal aeration system by using computational fluid dynamics (CFD) and the AHP-TOPSIS method. The quantitative and visual analysis of the airflow velocity, pressure, temperature, and RH was conducted using CFD on four different dryer aeration systems models, which were then ranked by preference value using the AHP-TOPSIS method. Model 4, with a sloping floor and circular pipe formation, was found to have the most optimal aeration system (preference value of 0.788) for a paddy grain deep bed dryer prototype.

1 Introduction

Drying is a crucial postharvest process for paddy grain which determines the quality of paddy grain and rice[1–3]. Paddy grain moisture content must be reduced from harvested rice with a moisture content of 22% to 30% to a moisture content of ⩽ 14% for safe storage to maintain quality[4]. This drying process must be done immediately after harvest, ideally within 12 to 24 h[5], especially in humid tropical climates[6]. Under high moisture content, paddy grains have an increased respiration rate due to enzyme activity and fungal growth, which can reduce the quality of the rice[7,8]. The drying process is influenced by various factors, such as moisture content, drying air temperature, relative humidity, and airflow rate[6,9,10]. Convective dryers stand out as an energy-efficient solution for drying bulky materials; these use hot-air drying media, a method employed in over 85% of industrial dryers[11]. However, limiting air heating to a temperature of < 45 °C can still achieve effective drying; this is considered as low-temperature drying. This approach is suitable for maintaining rice quality[12] and can increase the percentage of head rice yield[6,13]. One application of the convective drying method is deep or fixed bed drying[1,3], which uses airflow as a carrier of heat and moisture, the main parameters in the drying process. During the drying process, there is a moisture content gradient inside each layer, with the initial drying stage in the bottommost layer. As the drying air moves upwards, it permeates through the layer of particles and infiltrates the porous stationary medium[14,15]. Deep bed dryers allow the use of hot-air and ambient-air drying systems for grain drying, depending on the temperature and relative humidity (RH) of the drying air. Combining a good airflow control strategy with an appropriate aeration system is ideal for the development of effective and energy-efficient dryers. The aeration system used should be able to help the drying air spread evenly within the paddy grain pile.

In designing a dryer, a powerful analysis method is needed due to the number of alternative aeration systems. The aeration system discussed herein uses porous air pipes that provide voids within the grain pile as applied in an in-store dryer (ISD) for maize grains[16], with computational fluid dynamics (CFD) simulations for temperature, airflow and RH distribution in the ISD[17]. The CFD analysis is used to comprehensively overview airflow, temperature and pressure distribution in the drying chamber[17–21], which is the basis for selecting the aeration system used.

Simulating an aeration system with several operating conditions provides a complete picture of system performance. This is improved in the analysis, but it causes more criteria to be involved in determining the optimum aeration system. Thus, given that a selection method which accommodates all variables that affect the performance of the aeration system is needed, a multi-criteria decision-making (MCDM) analysis used to choose an aeration system used at the manufacturing stage. MCDM is widely used in various fields such as business, economics, manufacturing, and agriculture[22], fields related to irrigation[23–25], sustainable rural development[26,27], and agricultural machinery selection[28].

The analytical hierarchy process (AHP) is a comprehensive methodology developed explicitly for decision-making in MCDM. The method was developed by Saaty (1980) as a systematic approach to decision-making that considers various quantitative and qualitative criteria[29]. This technique formulates a problem as a hierarchy and allows viewing different quantitative and qualitative criteria for a problem. The AHP calculations involve a pairwise comparison matrix. Criteria and sub-criteria are subject to sensitivity analysis[30], and an optimal decision is obtained from a series of pairwise comparisons, assigning weightings to each factor based on influential factors and integrating the matrix obtained from pairwise comparisons[31].

The Technique for Order Preference by Similarity to an Ideal Solution (TOPSIS) is one of the best MCDM methods to rank alternatives due to its simple, fast, and systematic evaluation process[32]. It is an easily computable method and can represent the relative performance of decision alternatives in a simple mathematical form[33]. However, the standard TOPSIS approach is a deterministic method, where the weighted normalized decision matrix is developed by assigning random scalar values to various alternatives based on decision-maker preferences and the corresponding criteria. Thus, some decision results can be influenced by subjective preferences[34]. Therefore, the AHP-TOPSIS combination can provide more objective computation in the distribution of criteria weightings of alternatives.

This study aimed to analyze the optimum aeration system across four alternative designs of deep bed dryer models using CFD simulation and the AHP-TOPSIS method. The aeration system is evaluated based on the indicators of airflow uniformity, pressure, temperature, and RH inside the grain pile, which are simulated with CFD. The decrease in moisture content over time due to the effect of each aeration system was analyzed using the drying process simulation. The preference value of the optimum aeration system is determined using the AHP-TOPSIS method. The findings of this study offer a new perspective on thermal system design techniques, particularly in the context of aeration systems for grain dryers. The

innovative method and result proposed here can be a valuable tool for researchers and practitioners, especially those involved in drying agricultural products.

2 Materials and methods

2.1 Deep bed dryer model

The deep bed dryer model used in this analysis was developed from the ISD building model[16,17,35,36] with a modified aeration system, which combines different types of floor shape and air pipe formation (Fig. 1). The dryer had a diameter of 0.8 m and a height of 1.45 m with nine input pipes for air distribution (0.08 m diameter) four air output pipes (0.1 m diameter), square air inlet holes (0.2 m × 0.35 m) and air outlet holes (0.3 m diameter). The total capacity was 150 kg of grain with a density of 577 kg·m^{-3}.

The deep bed dryer models combined two floor shapes and two air distribution pipe patterns. The first floor was conical (Fig. 1(a)), which entered the plenum chamber with a grain unloading hole in the form of a circular opening in the middle of the plenum chamber. An unloading channel connected this unloading hole with the unloading door, which was in the plenum chamber wall at the bottom of the dryer. The second floor had a sloping shape (Fig. 1(b)) with a simple circular floor following the contour of the dryer wall, diagonally positioned at 35° to the x-axis, and the high part positioned above the blower and the low part opposite the direction airflow from the blower. A grain unloading hole was on the low side of the sloping floor and directly connected to the unloading door on the plenum chamber wall. The air distribution pipe consisted of nine air input pipes (0.08 m diameter) directly connected to the plenum chamber, as well as four air output pipes (0.12 m diameter) positioned floating in the grain pile (Fig. 1(a,b)). The input and output pipes had a rectangle pattern (Fig. 1(c)) and a circular pattern (Fig. 1(d)).

The combination of floor shape and air distribution pipe formation (Fig. 1) resulted in four distinct models of the deep bed dryer aeration system used in the CFD simulation. Model 1 had a conical floor and rectangle pipe formation (CFRP), Model 2 had a conical floor and circular pipe formation (CFCP), Model 3 had a sloping floor and rectangle pipe formation (SFRP), and Model 4 had a sloping floor and circular pipe formation (SFCP).

The Solidwork 2021 software[37] was used to draw the deep bed dryer model, which was then imported into the Ansys 2022 software[38]. Geometry preparation, and volume extract was done using Space Claim, followed by CFD simulation using Fluent. Also, the CFD simulation results were analyzed using contour images, vectors and graphs. The CFD output values included airflow velocity, pressure, temperature, relative humidity and the standard deviation of each model. The resulting data was analyzed using the AHP-TOPSIS hybrid method to determine the optimum aeration system of the four models analyzed.

2.2 CFD simulation

The CFD simulations are performed on the four dryer models with air input at three air speed levels (2, 2.5, and 3 m·s^{-1}). The

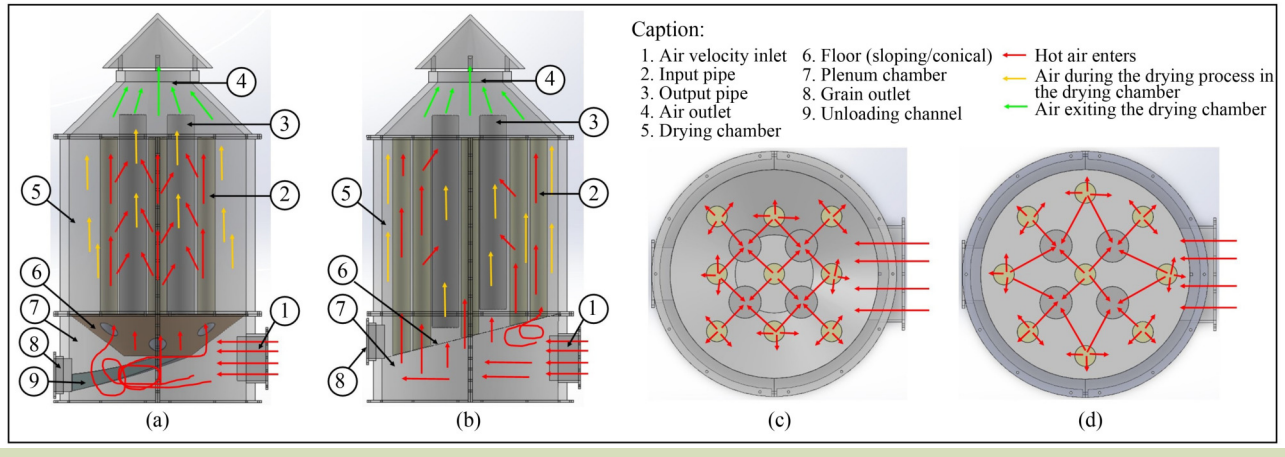

Fig. 1 Floor shape and air distribution pipe design of the deep bed dryer model: (a) conical floor shape, (b) sloping floor shape, (c) rectangular pipe formation, and (d) circular pipe formation.

air temperature at the inlet is 35 °C and it then passes through the heat exchanger such that the air is 40 °C upon entering the dryer. The paddy grain was a porous zone condition inserted in the drying chamber. Porous plates comprised the entire air distribution pipe and the floor of the dryer, and the walls of the dryer were under adiabatic conditions. The mesh used in the simulation was a polyhedra with sizes of 514,274 cells, 3,245,910 faces, and 2,537,876 nodes. This airflow simulation was performed under stable conditions as 10,000 iterations. Afterwards, the values, graph, contours, and distribution vectors of airflow velocity, pressure, temperature, and RH at various observation heights in the drying chamber were analyzed. The initial conditions, boundaries and materials involved in the simulation are presented in Table 1.

The CFD simulation procedure used in the Ansys software consists of three stages: preprocessor, solver, and postprocessor[39]. The preprocessor is the stage of modeling the research object in the form of geometry images in a format compatible with CFD software, the meshing process according to the design, followed by the application of boundary conditions and fluid properties. Then, the solver stage consisted of the core of problem-solving and CFD solutions. Calculations were performed with the conditions set in the preprocessor stage. The postprocessor stage was the final stage of CFD analysis producing the output and interpretation of simulation results as images, data, curves and animations. The CFD was applied to a finite volume for conduct a numerical analysis using three equations: mass equilibrium, momentum and energy[39].

The law of mass balance:

$$\frac{\partial(\rho u)}{\partial x}+\frac{\partial(\rho v)}{\partial y}+\frac{\partial(\rho w)}{\partial z}=0 \quad (1)$$

Table 1 Materials and boundary condition in the computational fluid dynamics simulation

Materials and boundary condition	Type	Parameter	Value
Paddy grain	Solid	Density	577 kg·m^{-3}
		Specific heat	2028 J·kg^{-1}·°C^{-1}
		Thermal conductivity	0.1223 W·m^{-1}·°C^{-1}
		Porosity	0.45 decimal
		Initial moisture content	25%
Wall (aluminum)	Solid	Density	2719 kg·m^{-3}
		Specific heat	871 J·kg^{-1}·°C^{-1}
		Thermal conductivity	2024.4 W·m^{-1}·°C^{-1}
Air	Inlet	Density	1.225 kg·m^{-3}
		Specific heat	1006.43 J·kg^{-1}·°C^{-1}
		Thermal conductivity	0.599 W·m^{-1}·°C^{-1}
		Viscosity	1 × 10^{-3} N.s·m^{-2}
Inlet	Fluid	Temperature	35 °C
		Velocity (3 level)	2, 2.5, 3 m·s^{-1}
		Air mass rate (3 level)	0.14, 0.175, 0.21 m^3·s^{-1}
		Turbulent intensity	5%
Heater (radiator)	Solid	Temperature	65 °C
Air enters the dryer	Fluid	Temperature	40 °C
Outlet (pressure outlet)	Fluid	Turbulent intensity	5%
Grain zone (porous zone)	Fluid	Viscous resistance (inverse absolute permeability) (1 m^{-2})	15.2 × 10^6 m^{-2}
		Inertial resistance	130 m^{-1}
		Porosity	45%
Air zone	Fluid	Default	
Wall	Solid	Adiabatic	

Momentum in x-direction:

$$\rho\left[u\frac{\partial u}{\partial x}+v\frac{\partial u}{\partial y}+w\frac{\partial u}{\partial z}\right]=\frac{\partial p}{\partial x}+\mu\left[\frac{\partial^2 u}{\partial x^2}+\frac{\partial^2 u}{\partial y^2}+\frac{\partial^2 u}{\partial z^2}\right]+S_{Mx} \quad (2)$$

Momentum in y-direction:

$$\rho\left[u\frac{\partial v}{\partial x}+v\frac{\partial v}{\partial y}+w\frac{\partial v}{\partial z}\right]=\frac{\partial p}{\partial y}+\mu\left[\frac{\partial^2 v}{\partial x^2}+\frac{\partial^2 v}{\partial y^2}+\frac{\partial^2 v}{\partial z^2}\right]+S_{My} \quad (3)$$

Momentum in z-direction:

$$\rho\left[u\frac{\partial w}{\partial x}+v\frac{\partial w}{\partial y}+w\frac{\partial w}{\partial z}\right]=\frac{\partial p}{\partial z}+\mu\left[\frac{\partial^2 w}{\partial x^2}+\frac{\partial^2 w}{\partial y^2}+\frac{\partial^2 w}{\partial z^2}\right]+S_{Mz} \quad (4)$$

Energy:

$$\rho\left[u\frac{\partial T}{\partial x}+v\frac{\partial T}{\partial y}+w\frac{\partial T}{\partial z}\right]=p\left[\frac{\partial u}{\partial x}+\frac{\partial v}{\partial y}+\frac{\partial w}{\partial z}\right]+k\left[\frac{\partial^2 T}{\partial x^2}+\frac{\partial^2 T}{\partial y^2}+\frac{\partial^2 T}{\partial z^2}\right]+S_i \quad (5)$$

Equation of state:

$$p=p(\rho,T) \text{ and } i=i(\rho,T) \quad (6)$$

$$\text{for perfect gas, } p=\rho RT \text{ and } i=CvT \quad (7)$$

where, ρ is air density, p is pressure, μ is viscosity, T is temperature, k is heat conductivity, R is the ideal gas constant, i is specific internal energy, Cv is air molecular heat, u, v, and w are momentum in directions x, y, and z, respectively, S_M is the source of momentum, and S_i is the internal energy source.

The grain drying process was simulated for 5 h in the four deep bed dryer models. The simulation used a discrete phase in transient CFD simulation[38] as the process of evaporation of moisture content from the grain pile. Changes in airflow velocity, temperature and RH were observed. Then, the moisture content in each observation layer was calculated using a thin-layer model in deep bed drying[40,41] involving moisture ratio and equilibrium equations:

$$MR=\frac{M-Me}{M_0-Me} \quad (8)$$

$$Me=\left[\frac{\ln\left(1-\frac{Pv}{Pvs}\right)}{-\mathrm{K}(T+\mathrm{C})100^{\mathrm{N}}}\right]^{\frac{1}{\mathrm{N}}} \quad (9)$$

where, MR is the moisture ratio, M_0 is the initial moisture content, M is the moisture content after drying duration, Me is moisture equilibrium, Pv is vapor pressure, and Pvs is saturated vapor pressure, the constants K, C, and N are 1.9187×10^{-5}, 51.161, and 2.445, respectively.

2.3 Determine the optimum model using the AHP-TOPSIS method

The optimal deep bed dryer model is determined through two stages: (1) calculates the criteria weightings for each alternative model using the AHP method, and (2) determines the preference value using the TOPSIS method (Fig. 2).

The AHP method is applied with the following steps: (1) creating a hierarchical structure (Fig. 2(b)), (2) creating a pairwise comparison matrix, (3) normalizing the matrix, and (4) calculating the eigenvector and maximum eigenvalue and tested its consistency. The computational process of the AHP method was:

$$\lambda_i=EV_i\left(\sum\nolimits_i a_{ij}\right) \quad (10)$$

$$\lambda_{max}=\sum\lambda_i \quad (11)$$

$$\mathrm{CI}=\frac{\lambda_{max}-n}{n-1} \quad (12)$$

$$\mathrm{CR}=\frac{\mathrm{CI}}{\mathrm{RI}} \quad (13)$$

where, EV_i is the eigenvalue of each criterion, $\lambda_{max}$is the maximum eigenvalue, n is the number of criteria, a_{ij} is the value at row i and column j of the pairwise comparison matrix, CI is the consistency index, CR is the consistency ratio, and RI is the random index, which in this research is 0.9 for n = 4 used for criteria and 1.24 for n = 6 used for sub-criterion[42].

The pairwise comparison matrix was deemed acceptable if the CR was $\leqslant$ 0.1. If the CR was > 0.1 (CR > 10%) then it was considered inconsistent. In such cases, weighing the importance of each element in the pairwise comparison matrix had to be repeated.

Preference values were calculated and decision made using the TOPSIS method by the following steps: (1) creation of a normalized decision matrix (Eq. (14)), (2) creation of a weighted normalized decision matrix (Eq. (15)), (3) determination of the matrix of positive and negative ideal solutions (Eq. (16)), (4) determination of the distance of each alternative to positive and negative ideal solutions (Eq. (17)), and (5) determination of the preference value for each alternative (Eq. (18)).

$$r_{ij}=\frac{X_{ij}}{\sqrt{\sum_{i=1}^{m}X_{ij}^2}} \quad (14)$$

$$y_{ij}=W_i\cdot r_{ij} \quad (15)$$

$$A^+=(y_1^+,y_2^+,\ldots,y_n^+) \text{ and } A^-=(y_1^-,y_2^-,\ldots,y_n^-) \quad (16)$$

$$D_i^+=\sqrt{\sum_{j=1}^{n}\left(y_{ij}-y_i^+\right)^2} \text{ and } D_i^-=\sqrt{\sum_{j=1}^{n}\left(y_{ij}-y_i^-\right)^2} \quad (17)$$

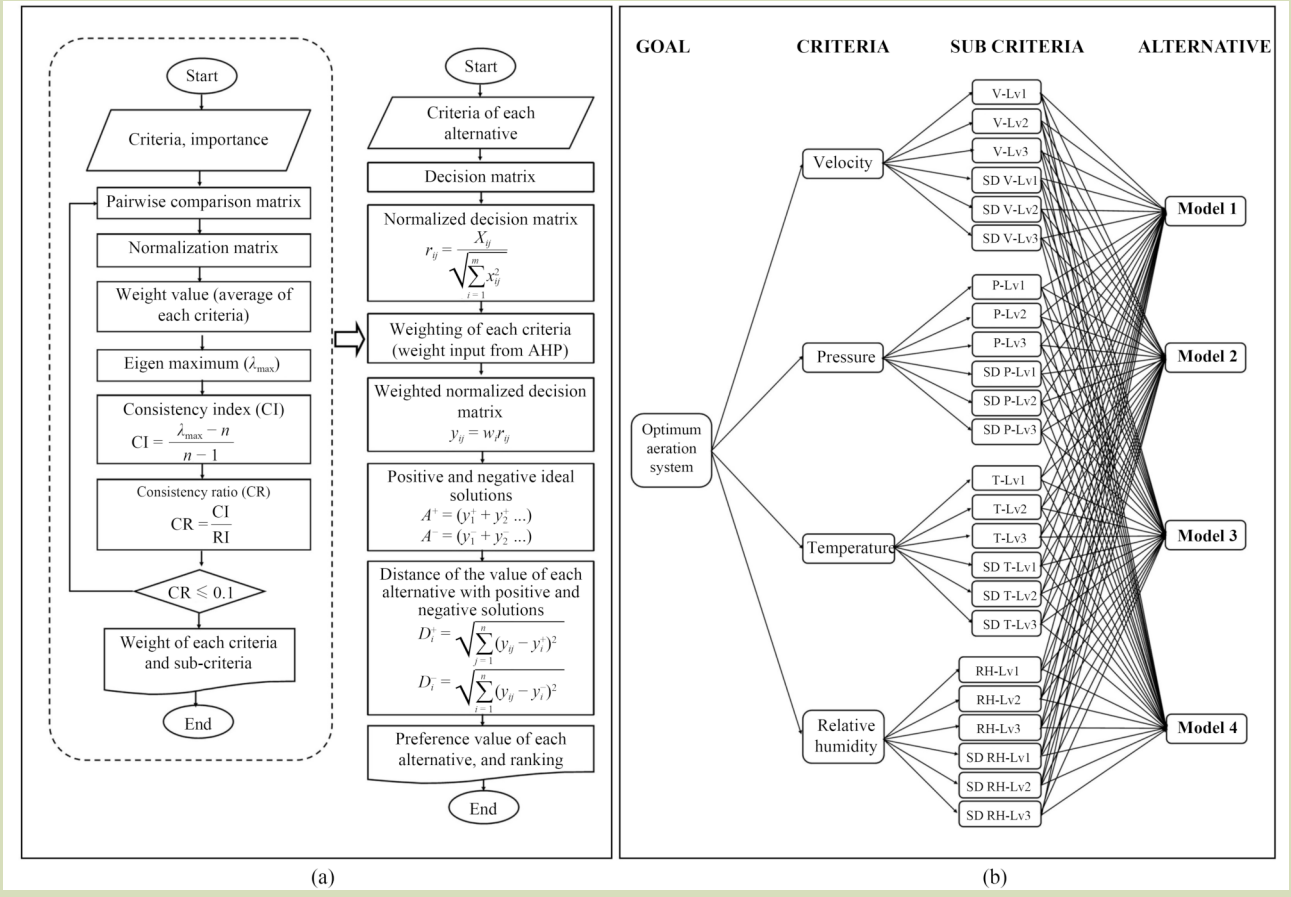

Fig. 2 Flowchart of the method in determining the optimum aeration preference of the deep bed dryer: (a) combination of the analytical hierarchy process and TOPSIS methods, and (b) AHP element for each of four models.

$$V_i = \frac{D_i^-}{D_i^- + D_i^+} \tag{18}$$

3 Results and discussion

3.1 Airflow velocity and vector

The airflow pattern in the drying chamber of the four deep bed dryer models appeared different, as presented in the airflow contour images (Fig. 3(a–d)). Models 1 and 2, which both had conical floors with grain unloading channels facing the direction of the air inlet, had obstructions to the incoming airflow, thus reducing the airflow velocity in the plenum chamber. However, the use of a circular pipe formation in Model 2 improve the flow distribution. The ample space (marked with dashed lines) in the flow vector above the air inlet and grain outlet in Model 1 indicated a weak range of airflow in the area. In Model 2, this occurs in the middle between the input pipes, which is evident in the airflow vector, in the vertical plane in the *y*-axis direction, and the horizontal plane in the *x*- and *z*-axes (Fig. 3(e,f)). Differences in drying airflow characteristics were evident in Models 3 and 4 (Fig. 3(g,h)), which had sloping floors with no obstacles in the plenum chamber, and thus the air was free to move in all directions before entering the floor pores and input pipes. The use of a rectangular pipe formation in Model 3 caused areas of the drying chamber to have weak flow coverage at the top of the air inlet and grain outlet (marked with dashed lines). In contrast, in Model 4, which had a circular pipe formation, there were no areas with weak airflow coverage, and thus there was more uniform flow distribution.

The flow dynamics inside the deep bed dryer started when the air entered the inlet and mixing occurs in the plenum chamber. The air then penetrated the porous floor and grain pile, which reduced air pressure due to resistance and friction with the floor pores and porosity of the grain. However, most of the air directly entered the input pipes inside the grain pile that covers all input pipes. The pressurized air pressed radially in all directions horizontally and entered the grain pile, then flowed

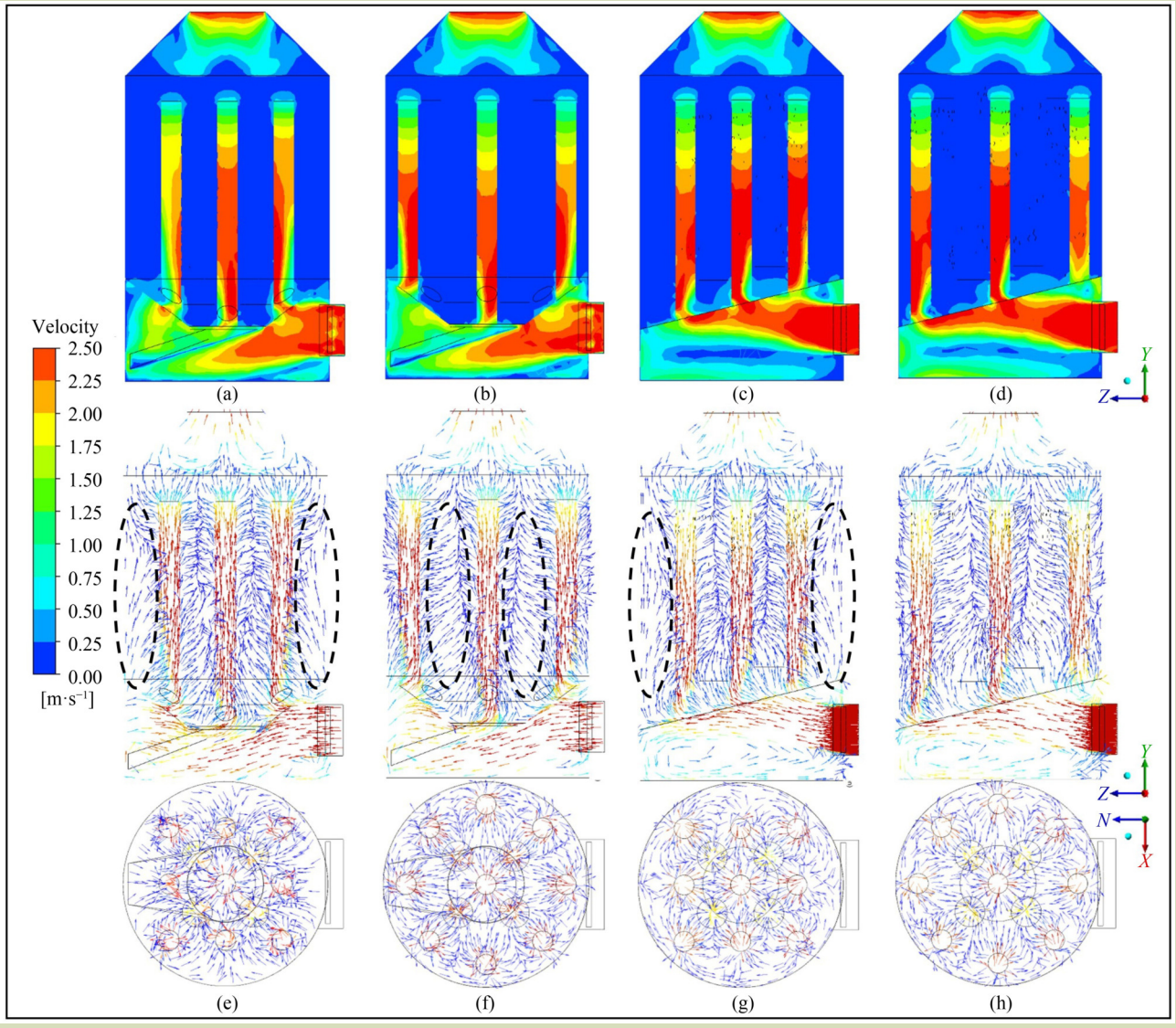

Fig. 3 Airflow velocity and vertical and horizontal plane vectors in each model of the deep bed dryer at an input air velocity level of 2.5 m·s^{-1}: (a) Model 1, (b) Model 2, (c) Model 3, and (d) Model 4, and airflow vectors in vertical and horizontal plane for (e) Model 1, (f) Model 2, (g) Model 3, and (h) Model 4.

toward the output pipes and moved freely toward the air outlet. The proportional arrangement of the input and output pipes made the air pressure range more uniform such that it flowed appropriately in and out of the grain pile.

The vertical distribution of airflow required high airflow velocity and pressure. Thus, to achieve a uniform distribution in the grain pile, it was necessary to maintain the stability of the inflow velocity, which was achieved using a sloping floor shape in Models 3 and 4. In contrast, the conical floor shape in Models 1 and 2 slowed airflow in the plenum chamber. Notably, uniformity in the horizontal flow direction was achieved with the radial pattern distribution pipe arrangement used in Models 2 and 4. This aeration pattern provided a proportional distance toward the outlet pipe so that air can flow properly from all areas toward the output pipe. The rectangle pattern used in dryer Models 1 and 3 created empty areas with a relatively large distance at four locations between the input pipe and the wall, such that the flow around the wall will weakened first before reaching the outlet pipes.

The floor shape and aeration pipe arrangement pattern both simultaneously affect the airflow direction vertically along the *y*-axis and horizontally along the *x*-axis and *z*-axis. As a

medium in heat and mass transfer, airflow distribution affected the distribution of pressure, temperature, and RH, so having a more uniform airflow distribution throughout the deep bed dryer area improved the drying process. Thus, airflow uniformity is essential in the design of convection dryer systems[43,44].

The airflow velocity in drying chambers of the four models at three input airflow velocity levels ranged from 0.007 to 0.597 m·s^{-1}. The most uniform airflow velocity distribution based on the minor standard deviation was found in Model 3, followed by Models 1, 4, and 2 (0.057, 0.059, 0.060, and 0.062 m·s^{-1}, respectively). The lowest standard deviation of air distribution occurred at Level 1 input air. Meanwhile, the highest variations were evident at Level 3 input air in Model 4, followed by Models 3, 2, and 1 (0.087, 0.089, 0.093, and 0.093 m·s^{-1}, respectively).

An increased input air velocity causes an increase in the variation of airflow in the drying chamber, albeit in small values, because the movement of this airflow occurred inside the grain pile as a porous zone. The change in airflow velocity along the *y*-axis in the drying chamber was similar across all models. Notably, the gradient of the responses (Fig. 4(e–h)) shows the response of the aeration system to the air input in distributing the flow in the drying chamber. All models had the same responses, where the airflow velocity decreased from 0.4 to 0.7 m along the *y*-axis and increased again to 1.2 m along the *y*-axis at all three air input levels.

Close responses for flow velocity levels for each model indicate a poor aeration system response. A more significant gradient of the velocity responses indicates a better aeration system response to the input airflow. For instance, the aeration system in Model 4 responds well to the given air input level, which increased the amount of distributed flow in the drying chamber as an effect of increasing the air input level. Table 2 presents the complete data for the average airflow velocity in the drying chambers, along with their standard deviation across the four models and three levels of input air velocity.

3.2 Airflow pressure

Input air velocity, floor porosity, air distribution pipes, grain

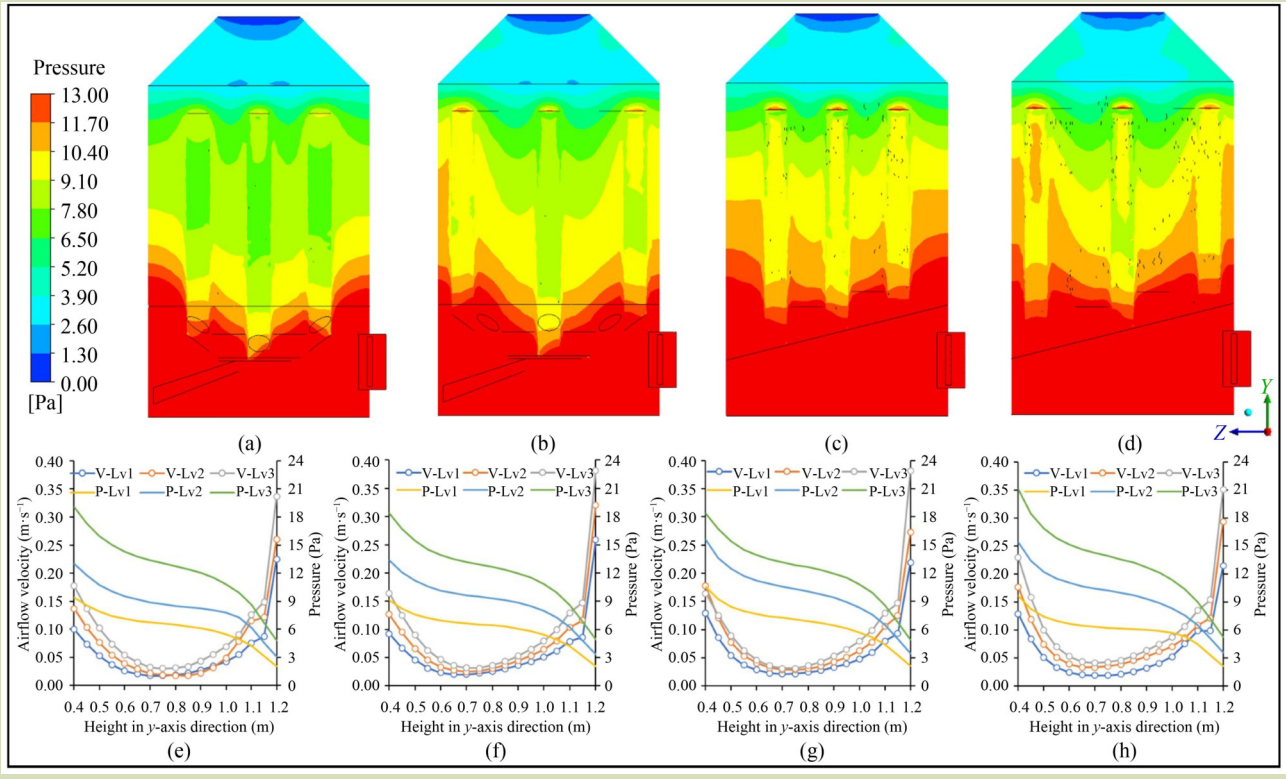

Fig. 4 Pressure contours of each model of deep bed dryer with an input air velocity level of 2.5 m·s^{-1} for (a) Model 1, (b) Model 2, (c) Model 3, and (d) Model 4, and velocity and pressure by height inside the drying chamber at the three input air velocity levels for (e) Model 1, (f) Model 2, (g) Model 3, and (h) Model 4.

Table 2 Average and standard deviation of airflow velocity, pressure, temperature, and relative humidity at each model and level of air input

Dryer model	Level of airflow input	Airflow velocity ($m \cdot s^{-1}$)		Pressure (Pa)		Temperature (°C)		Relative humidity (%)	
		AVG	SD	AVG	SD	AVG	SD	AVG	SD
Model 1	Level 1	0.06	0.06	6.19	1.88	39.09	0.70	44.93	1.72
	Level 2	0.07	0.07	8.47	2.45	38.39	0.58	46.65	1.47
	Level 3	0.09	0.09	12.43	3.63	37.90	0.50	47.90	1.31
Model 2	Level 1	0.06	0.06	6.09	1.78	39.20	0.71	44.67	1.73
	Level 2	0.08	0.08	8.92	2.54	38.49	0.58	46.40	1.48
	Level 3	0.10	0.09	12.24	3.41	37.99	0.50	47.67	1.30
Model 3	Level 1	0.06	0.06	6.63	2.08	39.35	0.41	44.30	0.97
	Level 2	0.08	0.07	9.73	2.99	38.59	0.35	46.13	0.86
	Level 3	0.10	0.09	12.24	3.41	37.99	0.50	47.67	1.30
Model 4	Level 1	0.06	0.06	6.07	1.76	39.35	0.38	44.30	0.91
	Level 2	0.08	0.07	9.66	2.92	38.60	0.31	46.10	0.78
	Level 3	0.11	0.09	13.25	3.93	38.07	0.33	47.44	0.85

zone porosity and grain zone height all affected the airflow pressure inside the deep bed dryer (Fig. 4). The four models simulated with CFD appeared to have different patterns of pressure change, as demonstrated by the pressure contours (Fig. 4(a–d)). The aeration system used in each model, which combined the shape of the floor and the formation of air distribution pipes, contributed to variations in the pattern and magnitude of air pressure. The four models had a significant pressure in the plenum chamber with a red color on the pressure contour. After the air penetrated the floor pore and grain zone, there was a pressure drop due to the increased height of the drying chamber.

The pressure distribution was better with a sloping floor shape compared to that with a conical floor shape. This is represented by the red area in the contour image after passing through the porous floor; it is more prominent on the sloping floor than on the conical floor. Subsequently, this was also influenced by the pipe formation; the circular pipe formation supports the pressure distribution better than the rectangular pipe formation. This is represented (Fig. 4(a–d)) by the color degradation of the pressure contour from red to brown, yellow, light green and green (high to low values).

The airflow input level affected the average pressure inside the drying chamber. A higher air input led to a greater pressure inside the drying chamber, and thus the pressure drop was more significant (Fig. 4(e,f)). The average pressure inside the drying chamber across the four models at three input air levels ranged from 6.07 to 13.3 Pa; the pressure loss in the four models for Levels 1, 2, and 3 airflow inputs was 7.6, 11.0, and 14.2 Pa, respectively.

The pressure distribution uniformity based on the minor standard deviation was best at Level 1 air velocity input with Model 4 had the least variability, followed by Models 2, 1, and 3 (1.76, 1.78, 1.88, and 2.08 Pa, respectively). The most variability was evident at the Level 3 air velocity input, which was greatest at Model 4, followed by Models 3, 2, and 1 (3.93, 3.41, 3.41, and 3.63 Pa, respectively). The uniformity data showed that the aeration system in Model 4 responded well to the air velocity input, such that the pressure changes in the drying chamber follow the changes in the level of air velocity input given, with the gradient of the response greater than the other models (Fig. 4(e–h)). Table 2 presents the overall data of the average pressure distribution and the standard deviation in the four models at three input air velocity levels.

3.3 Air temperature and RH

The air temperature distribution inside the deep bed dryer differs depending on the aeration system. The floor shape and formation of air distribution pipes significantly affect the uniformity of the temperature distribution (Fig. 5(a–d)). Models 1 and 2 had a significant difference in temperature distribution as evident in the contour image with the red area in the middle of the drying chamber and the brown and green areas filling a large contour area indicating a significant variation in temperature distribution. Better conditions were evident in Models 3 and 4, with more minor temperature

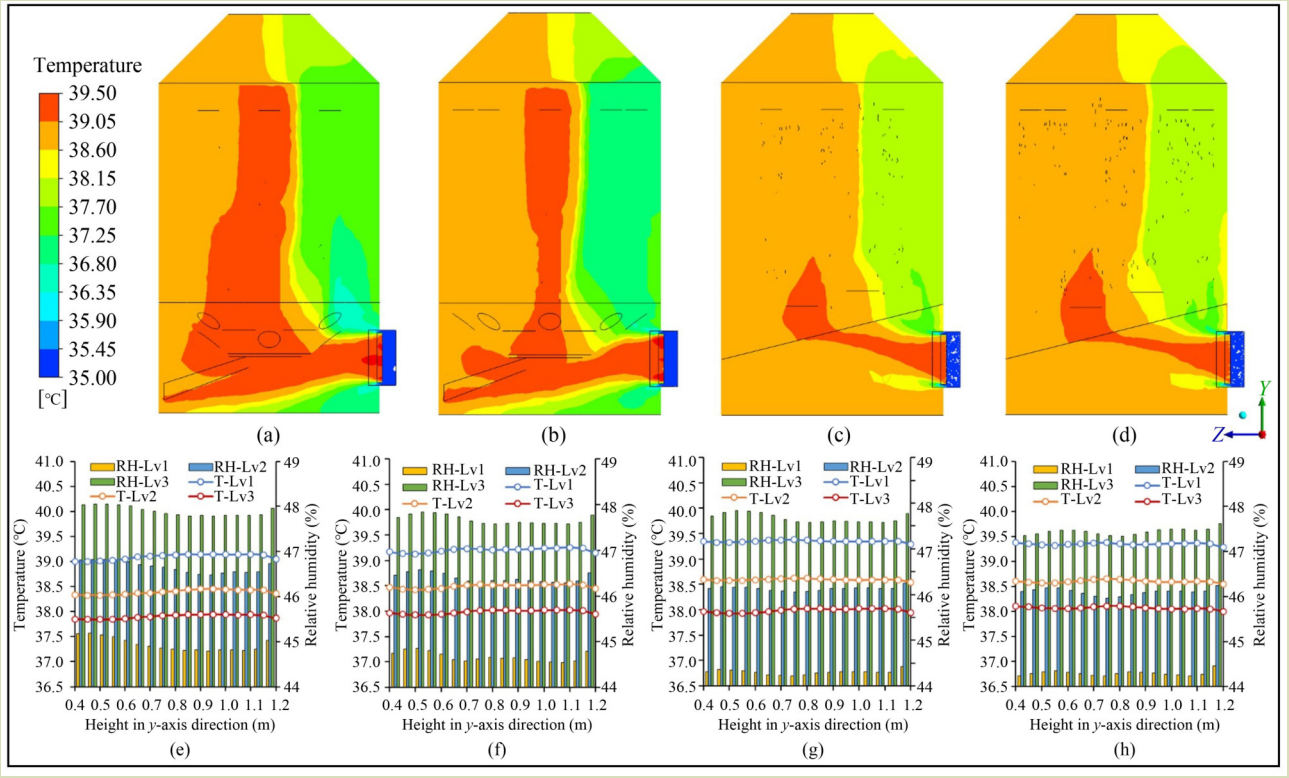

Fig. 5 Temperature contours at each model of the deep bed dryer with an input air velocity level of 2.5 m·s^{-1} for (a) Model 1, (b) Model 2, (c) Model 3, and (d) Model 4, and temperature and relative humidity by height inside in the drying chamber at the three input air velocity levels for (e) Model 1, (f) Model 2, (g) Model 3, and (h) Model 4.

variations with the red area only at the bottom of the drying chamber and most of the drying chamber area being brown, yellow and light green areas with slight differences in value.

On average, the air temperature inside the drying chamber of the four models decreased by 0.49 to 0.75 °C, with each increase in air velocity input level at a fixed temperature. The average temperature inside the drying chamber of the four models at three levels of input air velocity ranged from 37.9 to 39.4 °C, with the most uniform distribution in Model 4 Level 2, followed by Model 4 Level 3 and Model 3 Level 2 (deviation values of 0.31, 3.33, and 0.35 °C, respectively). The most significant variations in temperature distribution were evident in Model 2 Level 2, followed by Model 1 Level 1 and Model 2 Level 1 (deviation values of 0.58, 0.70, and 0.71 °C, respectively).

Based on the air temperature distribution (Fig. 5(e–h)), the air temperature tended to be stable, with minor changes alongside changes in the height of the drying chamber. The responses of Models 3 and 4 appear to be horizontal, indicating that the temperature distribution in the drying chamber was more uniform than that in Models 1 and 2. The average temperature and standard deviation data for the four models are presented in Table 2.

The RH distribution was inversely correlated with the temperature distribution pattern. When the temperature was high, the RH value become low and vice versa (Fig. 5(e–h)). The average RH value of the four models at three levels of air velocity input ranged from 44.3% to 47.9%, with Model 4 Level 2 having the most uniformity based on minor standard deviation, followed by Model 4 Level 3, Model 3 Level 2, and Model 4 Level 1 (0.87%, 0.85%, 0.86%, and 0.91%, respectively). On average, the RH of the air in the drying chamber increased by 1.25% to 1.83% with each increase in input air velocity level with a fixed temperature. The average RH and standard deviation data on the four models is presented in Table 2.

Air temperature is an essential variable in the drying process, followed by air velocity and grain pile height[45]. A greater water vapor capacity occurs with higher air temperature and low RH[2], and thus drying is faster. In a deep bed dryer with a

significant grain pile height, air pressure must also be considered to ensure that the airflow can penetrate the porosity of the grain and spread appropriately in the pile. Therefore, the function of the aeration system is crucial. Increasing the velocity of the incoming airflow can increase the pressure. However, with a fixed air input temperature, the effect becomes less significant with high airflow[2] because the temperature decreases in the drying chamber.

Providing a higher airflow input velocity must also be followed by efforts to increase the appropriate input air temperature in order to maximize the paddy grain drying conditions. Therefore, air velocity input needs to be controlled according temperature and RH levels during the drying process[35,46,47] in order to prevent over-drying and rewetting in the drying chamber. This can also conserve the heating energy of the air and blower used.

3.4 Drying process

The drying process in the four models (Fig. 6) was as follows. During the 5-h of drying simulation, all drying models had changes in moisture content, with a decreasing trend toward the upper layers. In contrast, the moisture content tended to increase in the upper layers of most deep bed dryers, especially during the initial drying period, due to the absorbed water vapor transported by the drying air from the previous layer, which can last longer under lower mass flow rates and deeper beds[48]. The deep bed dryer design with an aeration system could prevent significant variations in moisture content due to this fluctuation phenomenon, and thus the simulation results have a satisfactory outcome.

Each model had unique characteristics for the performance of its aeration system. Models 1 and 3 both had aeration pipes with a rectangular pattern. The moisture content at 40 cm decreased more than the other layers, as that layer was the lowest and was directly connected to the air supply from the plenum chamber. Due to the rectangular arrangement of the aeration pipes, air cannot flow more evenly to the layers above, and thus the gradient between layers was more evident. However, the gradient of the decreasing moisture content at 53, 80, and 107 cm was more evident in Model 1 (Fig. 6(a)) compared to Model 3 (Fig. 6(c)). This is likely to be due to Model 1 having a conical floor, which was an obstacle to the movement of drying air in the plenum chamber.

Model 3, which had a sloping floor, had a lower gradient due to better airflow in the plenum chamber and entering the input

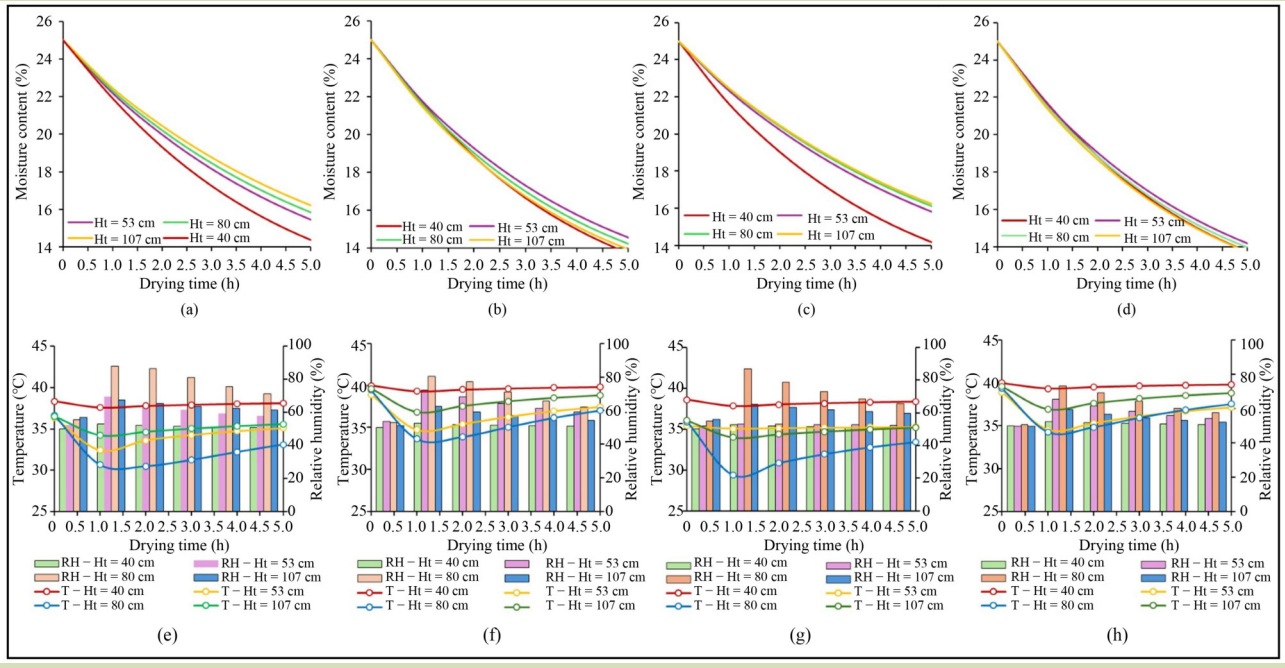

Fig. 6 Change of moisture content over time in the four deep bed dryer models with input air velocity rate of 2.5 m·s^{-1} for (a) Model 1, (b) Model 2, (c) Model 3, and (d) Model 4, and temperature and relative humidity during drying time for (e) Model 1, (f) Model 2, (g) Model 3, and (h) Model 4.

pipes. Nevertheless, the gradient at 40 cm and the layer above appeared more significant because this layer receives better air supply due to the sloping floor, and thus the moisture content dropped faster compared to the layers above. In the 5-h drying process, Model 1 had an average moisture content of 15.5% (range: 14.4% to 16.21%), with an average drying rate of 1.91% h^{-1}. This is influenced by the temperature range (average: 35 °C, range: 30.5 to 38.3 °C) and RH (average: 62.8%, range: 50.0% to 87.7%) during the drying process (Fig. 6(e)). Similarly, Model 3 was only able to achieve an average drying rate of 1.88% h^{-1}, with an average moisture content of 15.6% (range: 14.2% to 16.2%), temperature of 35.2 °C (range: 29.4 to 38.6 °C), and RH of 59.1% (range: 50.0% to 87.1%) (Fig. 6(g)).

Markedly different conditions occur in Models 2 and 4, which had a circular formation for their aeration pipes. These two models gave a better trend of decreasing moisture content than the other models, with a slight gradient between layers at all observation heights. The circular formation allowed for a better distribution of the drying air and RH in these two models. However, the reduction in moisture content differed between these models. Model 2, with a conical floor shape, had obstacles in the plenum chamber in the form of floor cones and unloading channels, thus inhibiting air movement. However, the aeration pipes were significant in improving the drying process in this model, with an average drying rate (Fig. 6(b)) of 2.18% h^{-1} and moisture content of 14.1% (range: 13.7% to14.6%). Also, this model had favorable temperatures (average: 37.6 °C, range: 33.6 to 40.0 °C) and RH (average: 59.8%, range: 50.0% to 80.4%) during the drying process (Fig. 6(f)).

Model 4 had a decreasing moisture content response that was favorable compared to the other three models (Fig. 6(d)). The gradient of the moisture content response at the four observation heights was quite small. This indicates that the difference in the drying rate between layers was not significant. The average drying rate in Model 4 was 2.22% h^{-1}, and thus within a drying simulation duration of 5 h, achieving an average moisture content of 13.9% (range: 13.7% to 14.2%) is possible. The average air temperature was 37.7 °C (range: 34.3 to 39.9 °C) and the average RH was 56.4% (range: 49.5% to 73.2%) (Fig. 6(h)). The drying process in Model 4 was as expected based on its design with the aeration system distributing air evenly across each layer in the deep bed dryer. The sloping floor freed the plenum chamber from obstacles, the drying air mixes properly, and the airflow penetrates the porous floor and the porosity of the grain. Additionally, the air input pipes also directed airflow into the pile properly. This input was also well supported by the air output pipes which serve as an outlet for moist air from inside the pile. The aeration system of Model 4 supplied drying air to all layers vertically and horizontally to prevent condensation in the grain pile, and thus the drying process proceeds efficiently.

3.5 Optimum aeration model

The weighting of the criteria was calculated using the AHP method, which includes velocity, pressure, temperature and RH, as well as the pairwise comparison matrix criteria. Normalizing these criteria resulted in an eigenvalue (λ_{max}) of 4.18, with a CI of 0.06 and CR of 0.07, The CR of $\leqslant$ 0.1 indicated that the criteria weightings were consistent. Additionally, sub-criteria weightings were also calculated for all air velocity input levels. A summary of the results of the calculation of criterion weights, sub-criterion weights, CI values, CRs, and final AHP calculation weights is presented in Table 3.

The weightings obtained by the AHP method (Table 3) and the CFD simulation output data from each model (Table 2) were analyzed using the TOPSIS method to identify the optimum aeration system model. By calculating the normalized matrix and the weighted normalized matrix, it was possible to calculate the distance of the positive and negative ideal solutions (D+ and D−) as well as the preference and ranking values presented in Table 4.

Based on the AHP-TOPSIS combination method analysis, there were differences identified in the performance of the aeration system based on the combination of floor shape and air distribution pipe formation. Model 1 (CFRP), with a conical floor shape and RP formation, had the lowest performance and ranked fourth, with a preference value of 0.18. Model 2 (CFCP), with a conical floor shape and CP formation, ranked third, with a preference value of 0.42. Model 3 (SFRP), with a sloping floor shape and RP formation, ranked second, with a preference value of 0.68. Finally, Model 4 (SFCP), with a sloping floor shape and CP formation, had the optimal aeration system performance, ranking first with a preference value of 0.79. Thus, the design of Model 4 was found to be the most suitable for developing a deep bed dryer with a combination of ambient air and hot air for drying paddy grain.

4 Conclusions

The overall CFD analysis at three airflow input levels revealed

Table 3 Criteria, sub-criteria, consistency index (CI), consistency ratio (CR), and final weight calculations

Criteria	Criteria weight	CI & CR of criteria	Sub criteria	CI & CR of sub-criteria	Sub-criteria weight	Final weight
Velocity	0.56	CI = 0.06 CR = 0.07	V-Lv1	CI = 0.06 CR = 0.05	0.42	0.24
			V-Lv2		0.20	0.11
			V-Lv3		0.12	0.07
			SD V-Lv1		0.15	0.08
			SD V-Lv2		0.08	0.04
			SD V-Lv3		0.04	0.02
Pressure	0.26		P-Lv1	CI = 0.03 CR = 0.02	0.37	0.10
			P-Lv2		0.19	0.05
			P-Lv3		0.14	0.04
			SD P-Lv1		0.16	0.04
			SD P-Lv2		0.09	0.02
			SD P-Lv3		0.05	0.01
Temperature	0.12		T-Lv1	CI = 0.08 CR = 0.07	0.45	0.05
			T-Lv2		0.19	0.02
			T-Lv3		0.12	0.01
			SD T-Lv1		0.12	0.01
			SD T-Lv2		0.08	0.01
			SD T-Lv3		0.03	0.004
Relative Humidity	0.06		RH-Lv1	CI = 0.08 CR = 0.07	0.45	0.03
			RH-Lv2		0.19	0.01
			RH-Lv3		0.12	0.01
			SD RH-Lv1		0.12	0.01
			SD RH-Lv2		0.08	0.005
			SD RH-Lv3		0.03	0.002

Table 4 The preference value of each model calculated by the TOPSIS method

Alternative	D+	D–	Preference	Rank
Model 1	0.019	0.004	0.18	4
Model 2	0.013	0.009	0.42	3
Model 3	0.007	0.015	0.68	2
Model 4	0.005	0.019	0.79	1

that Models 3 and 4 had acceptable uniformity in temperature and RH. Model 3 had the highest uniformity for velocity variables, followed by Models 1, 4 and 2, whereas Model 4 had the highest uniformity of pressure variables, followed by Models 2, 1, and 3. Each 0.5 $m \cdot s^{-1}$ increase in air velocity input decreased the average air temperature in the four models by 0.63 °C, as well as increasing the average RH, air velocity inside the drying chamber and pressure by 1.56%, 0.02 $m \cdot s^{-1}$ and 3.15 Pa, respectively. The best drying performance was seen in Model 4, with a drying rate of 2.22% h^{-1}; within 5 h, it can reach an average moisture content of 13.9%. The AHP-TOPSIS analysis revealed that Model 4 was the optimal aeration system, combining a sloping floor and a circular pipe formation to deliver the highest preference value of 0.79. This design is suitable for use in the development of a deep bed dryer for paddy grain.

Model 4 was the most optimal model through the implementation of a combination control system of ambient air and heating to stabilize the conditions of the input air. However, it will be necessary to test this models performance and validate the simulation model in an actual deep bed dryer. For this purpose, a system with a combination control algorithm should be designed to provide drying air volume that is appropriate for the environmental conditions and drying chamber.

Acknowledgements

This research was funded by Balai Pembiayaan Pendidikan Tinggi, Kemendikbudristek, and Lembaga Pengelola Dana Pendidikan (LPDP) through the Indonesian Education Scholarship (1083/J5.2.3/BPI.06/10/2021), and supported by Prof. Samsul Rizal of the Department of Mechanical and Industrial Engineering of Universitas Syiah Kuala in the application of Ansys software, which was funded by the LPDP and managed by Indonesian Science Fund (RISPRO/KI/B1/TKL/5/15448/2020).

Compliance with ethics guidelines

Diswandi Nurba, Sutrisno S. Mardjan, Dyah Wulandani, Loepold O. Nelwan, and I Dewa Made Subrata declare that they have no conflict of interest or financial conflicts to disclose. This article does not contain any studies with human or animal subjects performed by any of the authors.

REFERENCES

1. Firouzi S, Alizadeh M R, Haghtalab D. Energy consumption and rice milling quality upon drying paddy with a newly-designed horizontal rotary dryer. *Energy*, 2017, **119**: 629–636
2. Putra R N, Ajiwiguna T A. Influence of air temperature and velocity for drying process. *Procedia Engineering*, 2017, **170**: 516–519
3. Sarker M S H, Ibrahim M, Naziz N A, Salleh P M. Energy and rice quality aspects during drying of freshly harvested paddy with industrial inclined bed dryer. *Energy Conversion and Management*, 2014, **77**: 389–395
4. Thakur A K, Gupta A K. Two stage drying of high moisture paddy with intervening rest period. *Energy Conversion and Management*, 2006, **47**(18–19): 3069–3083
5. International Rice Research Institute (IRRI). Drying—IRRI Rice Knowledge Bank. Philippines: *IRRI*, 2013. Available at IRRI website accessed on April 27, 2024
6. Soomro S A, Chen K, Soomro S A. Mathematical modelling and optimisation of low-temperature drying on quality aspects of rough rice. *Journal of Food Quality*, 2020, **2020**: 1–10
7. Dillahunty A L, Siebenmorgen T J, Buescher R W, Smith D E, Mauromoustakos A. Effect of moisture content and temperature on respiration rate of rice. *Cereal Chemistry*, 2000, **77**(5): 541–543
8. Müller A, Nunes M T, Maldaner V, Coradi P C, Moraes R S, Martens S, Leal A F, Pereira V F, Marin C K. Rice drying, storage and processing: effects of post-harvest operations on grain quality. *Rice Science*, 2022, **29**(1): 16–30
9. Mihret Y C, Delele M A, Hailemesikel S T. Design, development, and testing of rice-husk fueled mixed-flow rice dryer for small-scale rice producer farmers. *Heliyon*, 2023, **9**(7): e18077
10. Jin Y, Wong K W, Wu Z, Qi D, Wang R, Han F, Wu W. Relationship between accumulated temperature and quality of paddy. *International Journal of Food Properties*, 2019, **22**(1): 19–33
11. Mujumdar A S. Handbook of Industrial Drying. Boca Raton: *CRC Press*, 2015
12. Genkawa T, Inoue A, Uchino T, Tanaka F, Hamanaka D. Optimization of drying condition for brown rice with low moisture content. *Journal of the Faculty of Agriculture, Kyushu University*, 2007, **52**(2): 381–385
13. Inprasit C, Noomhorm A. Effect of drying air temperature and grain temperature of different types of dryer and operation on rice quality. *Drying Technology*, 2001, **19**(2): 389–404
14. Silva D I S, Souza G F M V, Barrozo M A S. Heat and mass transfer of fruit residues in a fixed bed dryer: modeling and product quality. *Drying Technology*, 2019, **37**(10): 1321–1327
15. do Prado M M, Mazzini Sartori D J. Heat and mass transfer in packed bed drying of shrinking particles. In: El-Amin M, ed. Mass Transfer in Multiphase Systems and its Applications. *Intech Open*, 2011
16. Nelwan L O, Wulandani D, Widodo T W, Paramawati R. Energy Consumption and Cost of Drying of Hybrid Greenhouse Effect Dryer System and Integrated In-Store Dryer for Shelled Corn. In: Prosiding Seminar Nasional Teknik Pertanian 2008. Yogyakarta: *Perhimpunan Teknik Pertanian Indonesia*, 2008, 1–15 (in Indonesian)
17. Nurba D. Analysis of temperature, air flow, RH and water content distribution inside in-store dryer (ISD) for shelled corn. Dissertation for the Master's Degree. Bogor: *Institut Pertanian Bogor*, 2008 (in Indonesian)
18. Wulandani D. Study on temperature, RH and Air Flow Velocity Distribution of Dryer for the Design Optimization of Greenhouse Effect Solar Dryer. Dissertation for the Doctoral

Degree. Bogor: *Institut Pertanian Bogor*, 2005 (in Indonesian)
19. Olatunde G, Atungulu G, Sadaka S. CFD modeling of air flow distribution in rice bin storage system with different grain mass configurations. *Biosystems Engineering*, 2016, **151**: 286–297
20. Getahun E, Delele M A, Gabbiye N, Fanta S W, Demissie P, Vanierschot M. Importance of integrated CFD and product quality modeling of solar dryers for fruits and vegetables: a review. *Solar Energy*, 2021, **220**: 88–110
21. Iranmanesh M, Akhijahani H S, Jahromi M S B. CFD modeling and evaluation the performance of a solar cabinet dryer equipped with evacuated tube solar collector and thermal storage system. *Renewable Energy*, 2020, **145**: 1192–1213
22. El-Gayar O F, Leung P S. ADDSS: a tool for regional aquaculture development. *Aquacultural Engineering*, 2000, **23**(1-3): 181–202
23. Gómez-Limón J A, Martínez Y. Multi-criteria modelling of irrigation water market at basin level: a Spanish case study. *European Journal of Operational Research*, 2006, **173**(1): 313–336
24. Riesgo L, Gómez-Limón J A. Multi-criteria policy scenario analysis for public regulation of irrigated agriculture. *Agricultural Systems*, 2006, **91**(1–2): 1–28
25. Montazar A, Behbahani S M. Development of an optimised irrigation system selection model using analytical hierarchy process. *Biosystems Engineering*, 2007, **98**(2): 155–165
26. Zavadskas E K, Antucheviciene J. Multiple criteria evaluation of rural building's regeneration alternatives. *Building and Environment*, 2007, **42**(1): 436–451
27. Greening L A, Bernow S. Design of coordinated energy and environmental policies: use of multi-criteria decision-making. *Energy Policy*, 2004, **32**(6): 721–735
28. Nik M A E, Khademolhosseini N, Abbaspour-Fard M H, Mahdinia A, Alami-Saied K. Optimum utilisation of low-capacity combine harvesters in high-yielding wheat farms using multi-criteria decision making. *Biosystems Engineering*, 2009, **103**(3): 382–388
29. Darko A, Chan A P C, Ameyaw E E, Owusu E K, Pärn E, Edwards D J. Review of application of analytic hierarchy process (AHP) in construction. *International Journal of Construction Management*, 2019, **19**(5): 436–452
30. Petruni A, Giagloglou E, Douglas E, Geng J, Leva M C, Demichela M. Applying analytic hierarchy process (AHP) to choose a human factors technique: choosing the suitable human reliability analysis technique for the automotive industry. *Safety Science*, 2019, **119**: 229–239
31. Yaghoubi H, Allahyari M S, Firouzi S, Damalas C A, Marzban S. Identifying sustainable options for rice husk valorization using the analytic hierarchy process. *Outlook on Agriculture*, 2019, **48**(2): 117–125
32. Soni A, Chakraborty S, Das P K, Saha A K. Materials selection of reinforced sustainable composites by recycling waste plastics and agro-waste: an integrated multi-criteria decision making approach. *Construction & Building Materials*, 2022, **348**: 128608
33. Anupam K, Lal P S, Bist V, Sharma A K, Swaroop V. Raw material selection for pulping and papermaking using TOPSIS multiple criteria decision making design. *Environmental Progress & Sustainable Energy*, 2014, **33**(3): 1034–1041
34. Panda M, Jagadev A K. TOPSIS in Multi-criteria Decision Making: A Survey. In: 2nd International Conference on Data Science and Business Analytics (ICDSBA) 2018. Changsha, China: *IEEE Computer Society*, 2018, 51–54
35. Nurba D, Agustina R, Yasar M, Khurjannah A. Performance test of air input control system for paddy grain drying using in-store dryer. *IOP Conference Series. Earth and Environmental Science*, 2021, **922**(1): 012032
36. Nurba D, Agustina R, Zahara M. Study of changes in physical and chemical properties of corn during drying and storage process using a modified in-store dryer. *IOP Conference Series. Earth and Environmental Science*, 2021, **644**(1): 012016
37. Dassault Systèmes. What's new solidworks 2021? Massachusetts: *Dassault Systèmes*, 2021
38. Ansys, Inc. Ansys fluent tutorial guide. Canonsburg: *Ansys, Inc.*, 2022
39. Versteeg H K, Malalasekera W. An Introduction to Computational Fluid Dynamics: The Finite Volume Method. Harlow: *Pearson Education Ltd.*, 2007
40. Bala B K. Thin Layer Drying of Cereal Grains. In: Drying and Storage of Cereal Grains, 2nd ed. West Sussex: *John Wiley & Sons, Ltd.*, 2017, 107–145
41. Bala B K. Deep-bed and Continuous Flow Drying. In: Drying and Storage of Cereal Grains. 2nd ed. West Sussex: *John Wiley & Sons, Ltd.*, 2017, 147–194
42. Saaty T L, Vargas L G. Models, Methods, Concepts & Applications of the Analytic Hierarchy Process. Vol 175. New York: *Springer*, 2012
43. Kosasih E A, Zikri A, Dzaky M I. Effects of drying temperature, airflow, and cut segment on drying rate and activation energy of elephant cassava. *Case Studies in Thermal Engineering*, 2020, **19**: 100633
44. EL-Mesery H S, Tolba N M, Kamel R M. Mathematical modelling and performance analysis of airflow distribution systems inside convection hot-air dryers. *Alexandria Engineering Journal*, 2023, **62**: 237–256
45. Wincy W B, Edwin M, Sekhar S J. Optimization of process parameters to implement biomass gasifier for drying high moisture paddy in reversible flatbed dryer. *Energy*, 2022, **249**: 123771
46. Kjær L S, Poulsen M, Sørensen K, Condra T. Modelling of hot air chamber designs of a continuous flow grain dryer. *Engineering Science and Technology, an International Journal*, 2018, **21**(5): 1047–1055
47. Srzednicki G S, Hou R, Driscoll R H. Development of a control system for in-store drying of paddy in Northeast China. *Journal of Food Engineering*, 2006, **77**(2): 368–377
48. Ranjbaran M, Emadi B, Zare D. CFD simulation of deep-bed paddy drying process and performance. *Drying Technology*, 2014, **32**(8): 919–934